

THE X-RAY LUMINOSITY FUNCTION OF “THE ANTENNAE” GALAXIES (NGC4038/39) AND THE NATURE OF ULTRA-LUMINOUS X-RAY SOURCES

A. ZEZAS, G. FABBIANO

Harvard-Smithsonian Center for Astrophysics,
60 Garden Street, Cambridge, MA 02138

Draft version December 20, 2018

ABSTRACT

We derive the X-ray luminosity function (XLF) of the X-ray source population detected in the *Chandra* observation of NGC4038/39 (the Antennae). We explicitly include photon counting and spectral parameter uncertainties in our calculations. The cumulative XLF is well represented by a flat power law ($\alpha = -0.47$), similar to those describing the XLFs of other star-forming systems (e.g. M82, the disk of M81), but different from those of early type galaxies. This result associates the X-ray source population in the Antennae with young High Mass X-ray Binaries. In comparison with less actively star-forming galaxies, the XLF of the Antennae has a highly significant excess of sources with luminosities above 10^{39} erg s⁻¹ (Ultra Luminous Sources; ULXs). We discuss the nature of these sources, based on the XLF and on their general spectral properties, as well as their optical counterparts discussed in Paper III. We conclude that the majority of the ULXs cannot be intermediate mass black-holes ($M > 10 - 1000 M_{\odot}$) binaries, unless they are linked to the remnants of massive Population III stars (the Madau & Rees model). Instead, their spatial and multiwavelength properties can be well explained by beamed emission as a consequence of supercritical accretion. Binaries with a neutron star or moderate mass black-hole (up to $20 M_{\odot}$), and B2 to A type star companions would be consistent with our data. In the beaming scenario, the XLF should exhibit characteristic breaks that will be visible in future deeper observations of the Antennae.

Subject headings: galaxies: peculiar — galaxies: individual — galaxies: interactions — X-rays: galaxies

1. INTRODUCTION

It is well known that the Galaxy hosts a population of X-ray sources associated with X-ray binaries (XRBs) and supernova remnants (SNRs) (e.g. review in Watson et al. 1990; Grimm et al. 2001). Observations with the *Einstein* Observatory and later with ROSAT and ASCA, detected individual X-ray sources in nearby galaxies and initiated the study of the X-ray source populations in galaxies (e.g. Fabbiano 1989, Fabbiano 1995, Read et al. 1997; Wang et al. 1999; Yokogawa et al. 2000). X-ray Luminosity Functions (XLFs) were derived for a few galaxies (e.g. M31, M81, M101; Trinchieri & Fabbiano 1991, Fabbiano 1988, Fabbiano 1995, Primini et al. 1993, Supper et al. 2001, Wang et al. 1999), but these studies were of necessity limited by the available observational capabilities. Even so, it was clear that using samples of X-ray sources in external galaxies would reduce the problems in the study of the population properties of Galactic sources, inherent to our position in the Galaxy (Fabbiano 1995). Moreover, the XLFs reflect the formation, evolution, and physical properties of the X-ray source population in a galaxy, so comparison of XLFs of different galaxies, and modeling of the same, provide powerful tools for understanding the nature of the X-ray sources and relating them to the evolution of the parent galaxy and its stellar population.

With *Chandra* (Weisskopf et al 2000), X-ray source population studies are finally coming of age. The subarcsecond resolution of the *Chandra* mirrors (Van Speybroeck et al 1997) allows both the separation of discrete sources from surrounding diffuse emission and the detection of much fainter sources than previously possible. The

first *Chandra* studies of XLFs suggest trends related to the morphological type of the parent galaxy and/or the age of the prevalent stellar population: XLFs of early-type galaxies tend to have a break at the Eddington Luminosity of neutron star XRBs (e.g. Sarazin et al. 2001, Irwin et al. 2001, Blanton et al. 2001), while in the disk of M81, the XLF follows a single power-law (Tennant et al 2001). Similarly the XLFs of star-forming galaxies can also be modeled with a single power-law (e.g. Zezas et al. 2001; Bauer et al. 2001; Kilgard et al. 2001)

In this paper we report the study of the XLF of the X-ray sources detected in the Chandra observation of NGC 4038/39, the Antennae galaxies (OBSID 315; Fabbiano et al 2001, Paper I; Zezas et al 2001a and b, Papers II and III). Being a merging system of galaxies, the Antennae are undergoing exceptionally vigorous star formation (e.g. Whitmore et al. 1999), and thus provide a unique laboratory for the study of the X-ray source population in young and intense starbursts. The X-ray source population of the Antennae is exceptional, in that of the 43 point-like sources detected, 17 have X-ray luminosity significantly in excess of that expected from normal neutron star or stellar-mass Black Hole (BH) XRBs. These Ultra Luminous X-ray sources (ULXs) have spectra consistent with ULXs detected in other, more nearby galaxies (Paper III), but their number is exceptionally large.

Here we first derive the XLFs of the Antennae and discuss uncertainties and biases in its derivation (§2), and we compare it with the *Chandra* XLFs of other galaxies (§3). We then use these results, in conjunction with the spectral properties of the X-ray sources, and the informa-

tion on their optical counterparts presented in Paper III, to constrain models for the ULX population. Although the luminosities in Paper II were derived for $H_0 = 50 \text{ km s}^{-1} \text{ Mpc}^{-1}$, we use both $H_0 = 50 \text{ km s}^{-1} \text{ Mpc}^{-1}$ and $H_0 = 75 \text{ km s}^{-1} \text{ Mpc}^{-1}$ for the present discussion.

2. X-RAY LUMINOSITY FUNCTION (XLF) OF POINT SOURCES

2.1. *Derivation of the XLF*

In order to derive the XLF of the point sources in the Antennae we used the source list presented in Table 1 of Paper II, which contained 49 sources down to a limiting luminosity of $\sim 10^{38} \text{ erg s}^{-1}$ ($H_0 = 50 \text{ km s}^{-1} \text{ Mpc}^{-1}$; $\sim 5 \times 10^{37} \text{ erg s}^{-1}$, for $H_0 = 75 \text{ km s}^{-1} \text{ Mpc}^{-1}$). Of these, 31 (38, for $H_0 = 75 \text{ km s}^{-1} \text{ Mpc}^{-1}$) have luminosities below $10^{39} \text{ erg s}^{-1}$ while 18 (11) have higher luminosities. Forty-three sources appear point-like; of these 26 (33) have luminosities below $10^{39} \text{ erg s}^{-1}$ and 17 (10) have higher luminosities. The luminosities were calculated for a 5 keV bremsstrahlung model and Galactic column density ($N_{\text{H}} = 3.24 \times 10^{20} \text{ cm}^{-2}$; Stark et al. 1992) and are corrected for absorption. Fig. 1 shows the luminosity distribution of these sources. The calculation of an unbiased XLF from this luminosity distribution is not straightforward because of the spatial variations of the intensity of the diffuse emission in the Antennae galaxies (see Paper I; Fabbiano et al. 2001) which cause different detection thresholds over the system. To account for this effect without setting an overly conservative uniform completeness limit, and thus narrowing the luminosity coverage, we calculated a spatially-dependent correction function (CF, see §2.2), and corrected the XLF accordingly. This CF estimates the number of sources which escaped detection as a function of the source luminosity and the background surface brightness.

Given the limited source statistics, we calculated XLFs for sources detected in regions with just three background levels: 0.0 - 0.15 ct/pix (0.0 - 1.2 ct per typical detection cell; Paper II), 0.15 - 0.35 ct/pix (1.2 - 2.8 ct per detection cell) and greater than 0.35 ct/pix (2.8 ct per detection cell). These background levels were determined from the background map produced by the CIAO *wavedetect* tool, which is a reconstruction of the background based on the wings of the Mexican Hat function after subtracting all the point sources (Dobrzycki et al. 2000). The background levels were chosen in order to have at least 8 sources in each XLF. Fig. 2 shows the detected sources on the background map of the Antennae. On the same map we present as contours background levels of 0.01 cnts/pix, 0.15 cnts/pix and 0.35 cnts/pix. We also mark the detected sources following the notation of Table 1 from Paper II. In the calculation of the XLFs we did not include the extended sources (sources 5, 6, 7, 10, 24 and 29) and the Southern nucleus (the Northern nucleus is excluded as an extended source).

We also excluded the three hard sources which were detected in the obscured contact region between the two galaxies (sources 35, 39 and 40), because of the difficulty in correcting the LF for the effect of foreground obscuration which varies from source to source. The obscuration correction is further complicated by our ignorance of the three dimensional distribution of the X-ray sources and

the obscuring material. The latter is very hard to determine from the spectra of the sources, since it is unknown what fraction of the absorption is due to foreground material and what is due to intrinsic absorption in the source. The exclusion of these sources will not bias our XLF as the excluded area is very small compared to the total area of the Antennae. The hatched histogram in Fig 1 shows the luminosity distribution of the sources used for the determination of the XLF. The three uncorrected XLFs are shown in Fig. 3a.

2.2. *The Correction Function*

In order to determine the CF we simulated 50 realizations of three different datasets, one for each background level, with sources of luminosities in the range $10^{37} - 10^{39} \text{ erg s}^{-1}$. For these simulations we used the same spectrum as was used to calculate the luminosity of the sources (see §2.1). For the spectrum of the background we assumed a flat power-law as determined from spectral fits in a source free area of the ACIS-S3 chip. We ran *wavedetect* on each simulated dataset with exactly the same parameters as used for the source detection in the actual data. The 50 realizations give an uncertainty of 15-20% in the CF between the 100% and the 50% completeness limit, which is smaller than the Poisson error from the source counts.

The resulting CF is presented in Fig. 3b. The square points correspond to low background (0.1 cnts/pixel), the circles correspond to medium background (0.25 cnts/pixel) and the stars correspond to high background (0.45 cnts/pixel). The correction is important only for the lowest luminosity sources ($L_X < 1.6 \times 10^{38}$). The three curves differ close to the detection limit, the 50% completeness limit (indicated by a dashed line) ranges between $8 \times 10^{37} \text{ erg s}^{-1}$ and $1.3 \times 10^{38} \text{ erg s}^{-1}$ for all background levels. Since there are only 5 sources in this luminosity range, we can conservatively set our completeness limit at $1.3 \times 10^{38} \text{ erg s}^{-1}$.

The convolution of the three XLFs (presented in Fig. 3a) with the appropriate CF for each background (Fig. 3b) provides the completeness corrected XLF for each background level. This correction is important only in the luminosity range between the detection limit and $2 \times 10^{38} \text{ erg s}^{-1}$, where there are 7, 2 and 1 sources in the high, medium and low background XLFs respectively. Above this luminosity no correction needs to be applied (Fig. 3b). The corrected XLF is shown by the dashed line in Fig. 3a. Adding together the corrected XLFs gives the total XLF of the Antennae galaxies. The top left panel of Fig. 4 shows the differential total XLF whereas the top right panel shows the cumulative XLF. The errors in both plots are calculated according to the Gehrels statistic¹ (Gehrels 1986) and do not include uncertainties in the correction function. This XLF is complete down to $1.3 \times 10^{38} \text{ erg s}^{-1}$ which is the 50% completeness limit in the high background case. The application of the correction function and the 50% completeness will minimize the effect of the Eddington bias. Because of the applied corrections we cannot use the unbinned XLF for any further analysis.

2.3. *Uncertainties in the determination of the XLF*

¹ A modification of Gaussian statistics to approximate a Poisson distribution. The standard deviation of the Gaussian is $\sigma = 1 + \sqrt{0.75 + N}$.

The XLF as calculated above includes only errors associated with the Poissonian nature of the source detection process (source counting uncertainties). However, an XLF is also subject to uncertainties related to the determination of the luminosities for each source. These are: (i) the uncertainties in the count-rate of each source due to the Poissonian nature of the photon detection for each source (photon counting uncertainties) and (ii) uncertainties in the determination of the spectral shape of each source (spectral uncertainties). In order to determine the effect of these additional sources of error, we performed a Monte-Carlo simulation to obtain 1000 estimates of the count rate for each source. Although the photon detection process is governed by Poisson statistics, the use of Gaussian statistics is a fairly good approximation when dealing with sources with more than ~ 20 counts (e.g. Bevington & Robinson 1992). In this case the most appropriate determination of the standard deviation is given by the Gehrels formula (Gehrels 1986). Hence, in these simulations we used Gaussian deviates with mean equal to the number of detected counts and standard deviation given by the Gehrels statistic. The errors in the XLF due to photon counting uncertainties range from ± 0.2 for the high luminosity bins up to ± 2.0 sources in low luminosities.

From the simulated number of counts for each source we calculated the corresponding luminosity, corrected only for the Galactic N_{H} , for the best fit power-law model of the coadded spectra in the luminosity range of each source (presented in Paper III). In order to obtain an estimate of the uncertainties in the luminosity due to spectral uncertainties we also estimated luminosities for the above spectra, modified by the typical uncertainties in the photon indices and column densities for sources in each luminosity range given in Paper III: for fainter sources we used a steeper power-law with a larger range in the photon index and absorption. The spectral parameters used for these estimates are given in Table 1. To calculate the minimum luminosity we used the steepest slope with the highest absorption, whereas to calculate the maximum luminosity we used the flattest slope with the minimum absorption. The difference between the minimum and the maximum luminosity estimates for the same count rate is up to a factor of 2. This gives only the extreme values of the luminosity and may overestimate the uncertainties. A more accurate treatment should take into account the fact that the spectral uncertainties are also normally distributed and correlated, and perform a Monte Carlo simulation for the spectral parameters. However, this is quite complicated since the conversion factor from count rates to luminosity is not a linear function of the spectral parameters. The combined uncertainties due to photon statistics and spectral uncertainties range between 0.5 and 20.0 sources ($\sim 50\%$).

From the results of this simulation we derived the differential XLF by calculating the mean number of sources and the standard deviation for each luminosity bin using the same binning as for the observed LF presented in Fig. 4. For the cumulative XLF, we first constructed the cumulative XLF for each set of luminosity estimates. Then, we calculated the mean and the standard deviation of the number of sources in each bin. Since the two sources of errors (photon counting/spectral uncertainties for each source and number of sources in each luminosity bin) are

independent, we combined them in quadrature. The differential and cumulative XLFs calculated as described above are presented in the bottom left and right panels of Fig. 4 respectively.

A comparison between the XLFs shown in the top and bottom panels of Fig. 4 indicates that they are slightly different: a few sources in the second XLF have luminosities below our completeness limit and a hump present in the first XLF disappears in the second. This is mainly an effect of the intensity-dependent spectral models used to estimate the luminosities of the sources (Table 1), which causes lower luminosity sources to occupy lower luminosity bins than for the 5 keV Bremsstrahlung spectral model used in §2.2. From these figures is also clear that while the two XLFs have similar errors in the high luminosity bins (where errors are dominated by source counting statistics), in the lower luminosity bins the uncertainties of the second XLF are larger since the contribution of photon counting and spectral uncertainties is becoming important for fainter sources.

2.4. Fits to the XLF

We perform a Maximum Likelihood fit to the unbinned differential XLF following the method of Murdoch et al. (1973), which takes into account measurement errors. In order to be able to directly compare our results with results on other galaxies, we only include errors associated with the photon statistics for which we adopt the Gehrels approximation (Gehrels, 1986). We fit the XLF with a power-law of the form $\frac{dN}{dS} = A \times S^{-\alpha}$, where N is the number of sources and S is the number of counts for each source. For the exposure of this observation and a 5 keV thermal Bremsstrahlung model with Galactic line of sight absorption, 1 count corresponds to an absorption corrected luminosity of 10^{37} erg s $^{-1}$. We find a best fit slope of $-1.52^{+0.08}_{-0.33}$ (the errors are at the 90% confidence level; $\Delta \text{Log}(L) = 1.36$, where L is the likelihood function). Then from the number of detected sources with luminosities above our detection limit (12 counts or 1.2×10^{38} erg s $^{-1}$), we determine the normalization of the differential XLF to be $22.29^{+1.39}_{-0.32}$. To investigate the effect of the errors on this fit we also employed the method of Crawford et al. (1970) which is also a Maximum Likelihood method but it assumes no measurement errors. In this case we obtain very similar results but with smaller errors ($\alpha = 1.57 \pm 0.12$).

As a check of the above results we also fit the binned cumulative XLFs with the *Sherpa* fitting package (Freeman et al. 2001), which is part of the CXC-CIAO tool suite. We assumed a power-law of the form $N(> L_X) = B \left(\frac{L_X}{10^{38} \text{ erg/s}} \right)^{-\beta}$, where $\beta = \alpha - 1$ and we used the Cash statistic (Cash 1979), because in the highest luminosity bins there are very few sources and the errors cannot be described by Gaussian statistics. Using the XLF of Fig 4b which includes only source counting errors gives a slope of $\beta = 0.47^{+0.05}_{-0.05}$ and a normalization $B = 46.12^{+4.4}_{-4.0}$. The cumulative XLF together with the best fit model and the residuals after the fit are shown in Fig. 4b. The errors are at the 90% confidence level; $\Delta \text{Log}(L) = 1.36$, where L is the likelihood function. The shape of the XLF suggests that there may be a break around 10^{39} erg s $^{-1}$. However, fits with a broken power-law could not be justified

by the existing data, since the improvement in the fit is not statistically significant.

A fit of the cumulative XLF which also includes errors due to photon and spectral uncertainties (Fig. 4d) with the same model gives very similar results and the best fit slope is $0.45^{+0.05}_{-0.05}$. The normalization is $B = 38.9^{+3.9}_{-3.8}$. The best fit model and the resulting residuals are shown in Fig. 4d. Since this is the most accurate determination of the parameters of the XLF, we will use these results in our analysis.

Although we find that the two methods for the determination of the errors in the XLF give very similar results, for XLFs with larger number of sources, the standard Poissonian (or Gehrels) errors may underestimate the real uncertainties, especially for the lowest luminosity bins. This is because given the shape of the XLF, there are larger numbers of sources in the lower luminosity bins and therefore smaller errors if only source counting uncertainties are assumed. However, fainter sources have larger photon counting and spectral uncertainties which may well dominate over the source counting errors. Therefore both sources of uncertainty should be taken into account in the derivation of the XLF.

3. DISCUSSION

In the previous section we have derived the XLF of the discrete sources in the Antennae galaxies. Now we will use these results, together with the spectral and multiwavelength properties of the sources presented in Paper III, in order to constrain the nature of these X-ray sources. We will focus on the enigmatic ULX source population ($L_X > 10^{39}$ erg s $^{-1}$, well above the Eddington luminosity of a spherically accreting neutron star) which is uniquely rich in the Antennae. A discussion on the nature of the lower luminosity sources was presented in Paper III, where we concluded that they were likely to be similar to well-known Galactic sources.

3.1. Luminosity function

The shape of the Luminosity Function of the X-ray source population in a galaxy can provide constraints on the nature of the sources. For example, theoretical modeling by Wu (2000) suggested that the aging of the X-ray source population and successive bursts of star-formation may produce discontinuities in the XLF. Constraints on the evolution and the nature of the X-ray sources can also be set by comparing the XLFs of galaxies in various evolutionary stages. The cumulative XLF of the Antennae galaxies is well fit with a single power-law with a slope of $\alpha = -0.45$. This is much flatter than that found in the bulge of M31 ($\alpha = -0.8$ Trinchieri & Fabbiano 1991) or other early type galaxies in the same luminosity range (e.g. NGC4697 where $\alpha = -0.29$ for $L_X < 3.2 \times 10^{38}$ erg s $^{-1}$ and -1.76 for $L_X > 3.2 \times 10^{38}$ erg s $^{-1}$; Sarazin et al. 2000), for the same formalism of the XLF. However, the measured slope is similar to the XLF of M82 (Zezas et al. 2001) and of the disk population of M81 ($\alpha = -0.5$) (Tennant et al. 2001). It is also similar to the slope of the HMXB population of our Galaxy as measured by Grimm et al. (2001). A comparison between the XLF of the Antennae with that of other galaxies is given in Fig. 5, where we see that the XLFs of galaxies with some

level of star-formation do not show the break reported in early type galaxies. In Figure 6 we plot the logarithm of the normalization of the XLF (at 10^{38} erg s $^{-1}$) against its slope for star-forming and early-type galaxies (for the early type galaxies we use the slope of the high end of the XLFs, $L_X > 10^{38}$ erg s $^{-1}$). In this plot we clearly see that star-forming galaxies are well separated from more evolved systems. The difference in the normalizations is most probably related to the stellar content of the systems (although as pointed out by Grimm et al. (2001) the XLF of a galaxy is not a secure measure of its star-formation rate). The same effect is seen when we compare the slopes of the XLFs with the U-B colours and H $_{\mathrm{I}}$ surface density of the galaxies. The former gives a measure of recent star-formation, since is very sensitive on the number of early type stars. However, the U-B index is also sensitive to obscuration which makes it very difficult to use as an accurate star-formation indicator. The H $_{\mathrm{I}}$ surface density instead is directly related to the surface density of the star-formation rate by the Schmidt law (e.g. Kennicutt, 1998). This star-formation indicator also suggests that more actively star-forming galaxies have flatter XLFs than early type galaxies. A more thorough investigation of this effect including galaxies with intermediate activity levels is presented in Kilgard et al. (2001, in prep.; see also Prestwich, 2001).

The difference between the XLF of early-type galaxies and star-forming galaxies appears to be related to their stellar populations. X-ray sources in E and S0 galaxies as well as in bulges of spiral galaxies (eg M31, M81) are likely to be XRBs with a low mass (later than G type) companion (LMXBs), since this is the dominant stellar population in early type galaxies. These systems become active after the donor star fills its Roche lobe, an event which takes place $\sim 0.1 - 1$ Gyr after the formation of the binary (eg Verbunt & van den Heuvel 1995). Instead, in star-bursting galaxies, of which the Antennae are an example, the X-ray source population, while including an older LMXB component, is likely to be dominated by luminous 'young' short lived sources: X-ray binaries with O and B type companions (HMXBs) and luminous SNRs, since early type stars are the dominant stellar population.

In the Milky Way, SNRs and most HMXBs are not observed at luminosities above 10^{38} erg s $^{-1}$ (e.g. Grimm et al. 2001). In the Antennae instead, and to a lesser degree in M81 and M82 (which host lower level star-formation activity) we observe a large number of ULXs (Fig. 5). This excess holds even if we use luminosities calculated for $H_0 = 75$ km s $^{-1}$ Mpc $^{-1}$ (dashed line in Fig. 5). The increasing numbers of ULXs with increasing starburst activity associates these sources with a young stellar population. If the break in the XLF of early type galaxies is the reflection of the mass of the accretors in the XRB population (Sarazin et al. 2000), the flat XLF of star-forming galaxies might suggest a radically different accretor mass function or XRBs with significantly different emission properties.

In what follows we discuss possibilities for the nature of the ULXs, in the light of the XLF and their spectral and multiwavelength properties presented in Paper III.

3.2. The nature of the ULXs

Extranuclear ULXs with luminosities in excess of 10^{39} erg s $^{-1}$ and as high as $\sim 10^{40}$ erg s $^{-1}$, were known from previous studies with *Einstein*, ROSAT and ASCA (e.g. Fabbiano et al. 1995; Roberts & Warwick, 2000, Colbert & Mushotzky 1999, Makishima et al. 2000). The most extreme example is the source recently discovered in the central region of M82, which reaches luminosities higher than 10^{40} erg s $^{-1}$ (Kaaret et al. 2001, Matsumoto et al. 2001). ULXs are known to vary and tend to have hard spectra which can be well modeled with a multi-temperature disk black body model (disk-BB) with a temperature of $\sim 1 - 2$ keV (e.g. Zezas et al. 1999; Makishima et al. 2000). Also, some of them experience hard/low - soft/high transitions typical of black hole candidate binaries (Kubota et al. 2001; La Parola et al. 2001). As discussed in Paper III, 3 of the ULXs in the Antennae are variable and their X-ray spectra are consistent with the models described above.

Two scenarios have been advanced to explain the high luminosities of ULXs: the first, which has been widely discussed in the literature, is that of accretion binaries with a BH of mass in the range $10 - 1000$ M $_{\odot}$ (intermediate mass black-holes; IMBHs) (e.g. Fabbiano et al. 1995; Marston et al. 1995; Ptak & Griffiths 1999; Matsumoto et al. 1999; 2001; Zezas et al. 1999; Makishima et al. 2000; Kubota et al. 2001). The second model, is that of a binary system with beamed emission and does not require high mass accretors (Reynolds et al. 1997; King et al. 2001). Below we will discuss how these models measure against the observations of the ULXs in the Antennae galaxies.

3.2.1. Intermediate Mass Black holes (IMBHs)

Because of the high disk-BB temperatures suggested by the data, in IMBH models ULXs are explained by either accretion onto rotating BHs (Makishima et al 2000) or by the presence of ‘slim’ accretion disks around the BH (Watarai et al. 2000). Formation scenarios for the ULXs include first the formation of the IMBH, either by merging of stars in a cluster (Portegies Zwart et al. 1999) followed by direct collapse into a IMBH (Arnett 1996), formation of a massive object in the core of a dense cluster (Portegies Zwart & McMillan 2002), by merging of smaller BHs in a cluster (Taniguchi et al 2000), or as the result of the evolution of primordial population-III stars (Madau & Rees 2001). Once the IMBH exists, the ULX may form by capture of a normal star (Fabian et al 1975, Quinlan & Shapiro 1990, Madau & Rees, 2001).

While any of these scenarios may explain an isolated instance of ULX, some of their predictions are hard to reconcile with the properties of the ULX population of the Antennae galaxies. In what follows, we discuss these constraints for each model:

(1) The Portegies Zwart et al (1999) scenario would produce IMBHs via stellar collisions (and then ULXs by capture) in young stellar clusters. However, the position of most of the Antennae ULXs is near but not coincident with such clusters (typical offsets are $\sim 100 - 300$ pc; Paper III). As discussed in Paper III, this lack of positional coincidence may suggest that the ULXs are runaway bina-

² The rate for such captures is proportional to the stellar density: $r = 2\pi 3.15 \times 10^{-24} \left(\frac{X}{R_*}\right) \left(\frac{R_*}{R_{\odot}}\right) \left(\frac{\rho}{\text{pc}^{-3}}\right) \left(\frac{M+M_*}{M_{\odot}}\right) \left(\frac{v_d}{\text{km/s}}\right)^{-1} \text{s}^{-1}$ (Fabian et al. 1975, Quinlan & Shapiro 1990), where M_* and R_* are the mass and the radius of the star respectively, ρ is the density of the cluster, X is the capture radius, v_d^2 is the stellar velocity dispersion and M is the mass of the compact object.

ries. This hypothesis is explored further in §3.2.3, where we derive mass constraints for such a system that exclude IMBHs.

Even if they receive kicks, massive remnants would be expected to return to their parent cluster within a few crossing times (Portegies Zwart et al. 1999). This timescale is of the order 10^5 yr for the cluster R136, the dominant cluster in 30Dor in the LMC. The stellar clusters in the Antennae are at least 10 times more massive than R136 (Whitmore et al. 1999), resulting in an even shorter return timescale ($t \propto M^{-1/2} r^{3/2}$, where M is the mass of the cluster and r is its half-mass radius; Portegies Zwart et al. 1999). Therefore, one expects only to find massive objects in stellar clusters or close to the nuclear regions of galaxies, in contrast to what we see in the Antennae.

(2) As mentioned by Portegies Zwart & McMillan (2002), isolated IMBHs may be the remnants of evolved (and therefore dissolved) dense star clusters. However, the typical masses for the young star-clusters in the Antennae ($10^4 - 10^6$ M $_{\odot}$; Zhang et al. , 2001) imply relaxation timescales which would prevent core collapse and formation of IMBHs (Portegies Zwart & McMillan 2002).

(3) In the Taniguchi et al (2000) model, the IMBHs formation timescale is ~ 1 Gyr. In this model, the IMBHs would be likely to be found in globular clusters or galactic nuclei. Clearly this model does not predict the preferential association of ULXs with actively star-forming galaxies, shown by the comparison of galaxian XLFs (§3.1.).

(4) In the Madau & Rees (2001) model, the IMBHs would eventually drift into globular clusters or nuclei because of dynamical friction. However, the time scale for this process is long enough ($\sim 10^3$ Gyr for a 150 M $_{\odot}$ black-hole, 1 kpc from the nucleus) that we could observe some of these IMBHs while they drift through the galaxy after having captured a companion star in a dense star cluster. The capture timescale is proportional to the stellar density of the cluster ², hence the required density for a capture timescale of 50 Myr (the typical age of the optical counterparts of the ULXs in the Antennae) is $\sim 3 \times 10^5$ pc $^{-3}$. Indeed, in some star clusters in starburst regions such high densities can be found (e.g. Massey & Hunter 1998). So, at this moment, this model is still a possibility for the ULXs in star-forming galaxies.

Both the Taniguchi and the Madau & Rees models may be relevant for ULXs in E and S0 galaxies, where these sources may be associated with globular clusters (e.g. Angelini et al 2001). The relative paucity of ULXs in early-type galaxies (see Fig. 5) cannot be due to the effect of dynamical friction, since the timescales are much larger than the ages of star-clusters in these galaxies and the high stellar densities would foster the formation of many LMXB-IMBH systems. It is also unlikely that it may be connected with short life-times for these sources. Even if accretion rates scale with the mass of the IMBH, resulting in 100-times higher rates than in LMXB-BH Galactic binaries, we would still expect these binaries to live $10^5 - 10^6$ yr after they enter their X-ray emitting phase, which begins $\sim 10^8$ yr after their formation. Instead, the lack of ULXs

in early-type galaxies may suggest that ‘potential’ ULXs with low mass companions are X-ray transients with very long recurring timescales. Indeed, black-hole binaries with evolved companions are expected to form soft X-ray transients (King et al. 1996). Another possibility is that these systems went through a thermal timescale mass transfer episode resulting in a common envelope situation (e.g. King et al. 2001). In this case the X-ray binary is not observable because the X-ray emission is attenuated by the high density material (see next paragraph).

3.2.2. Super-Eddington accretion and beaming

An alternative model for the ULXs is that they are beamed X-ray binaries, with normal mass accretors (neutron star or stellar mass BH). There are two cases of beaming which can apply to ULXs : relativistic beaming from a jet (e.g. Reynolds et al. 1997), and anisotropic emission from an accretion disk in a supercritical accretion regime (e.g. King et al. 2001). Examples of relativistically beamed sources would be the elusive microblazars (e.g. Mirabel & Rodriguez 1999). In the case of microquasars, which also exhibit relativistic jets, is unlikely that the bulk of their X-ray emission is relativistically beamed (at least while in high state; see Fender (2001) for the contribution of jets in the low state), since their X-ray spectra clearly show signatures of emission from an accretion disk (e.g. Miller et al. 2001; Makishima et al. 2000), which otherwise would be outshined by the jet. Similarly, since the coadded spectra of the ULXs in the Antennae suggest emission from an accretion disk (see Paper III) most probably the bulk of the X-ray emission in most of these sources is not relativistically beamed. Recently Kording et al. (2001) by modeling the composite XLF of three nearby galaxies (M31, M101, M82) with a population of X-ray binaries with jets, constrained the contribution of the jet to 30% of the emission of the disk. This contribution is in general agreement with the disk dominated X-ray spectra of microquasars and ULXs, but it requires a jet component which should be visible in high quality spectra. This could be associated with the power-law component detected in these sources

The relativistic beaming factor b for a given Lorentz factor γ (and the corresponding $\beta = u/c$) is a function of the angle θ between the jet axis and the line of sight: $b = [\gamma(1 - \beta \cos\theta)]^{-p}$, where p depends on the parameters of the jet (a reasonable value is 4; e.g. Urry & Shafer, 1984; Mirabel & Rodriguez 1999). From this formula one derives a maximum beaming factor is $\sim (2\gamma)^p$ for a pole-on view of the jet. Assuming that the most luminous source in the Antennae is beamed with the maximum beaming factor, we can estimate the viewing angle for the least luminous source detected in our observation, assuming that both belong to the same parent population and the luminosity difference is just an orientation effect :

$$\frac{L_{max}}{L_{min}} = \left(\frac{b_{max}}{b}\right) = [2\gamma^2(1 - \beta \cos\theta)]^p \quad (1)$$

From this equation, for the measured luminosity ratio of 120, and values of $\gamma = 3$ ($\beta = 0.92$, beam solid angle 0.1 sr) and $\gamma = 5$ ($\beta = 0.98$, beam solid angle 0.04 sr) (e.g. Mirabel & Rodriguez 1999) we obtain viewing angles of 30° and 18° respectively. Assuming random orientation of the jets on the sky, the ratio between maximally beamed

sources and sources with lower beaming factors due to different orientation is equal to the ratio of their beam solid angles. This predicts 8 sources, down to our limiting luminosity ($\sim 10^{38}$ erg s $^{-1}$), for each beamed source for both values of γ . Therefore for the 4 sources above 10 40 erg s $^{-1}$, we expect to have 32 sources down to our detection limit. This is more than 75% of the total observed population and may agree with the model of Kording et al. (2001).

Anisotropic emission is a natural consequence of thick accretion disks (e.g. Abramowicz et al. 1980, Madau 1998), which are consistent with the X-ray spectra of ULXs (e.g. Watarai, et al. 2000; Kubota et al. 2001). In this case the luminosity enhancement is not due to relativistic effects (Lorentz boosting) as in the case of jet dominated sources, but to emission from the inside walls of the funnel, which is believed to form in the inner part of thick accretion disks (e.g. Abramowicz et al. 1980). This beaming was invoked by King et al. (2001) in order to explain the large number and high observed luminosities of ULXs in the Antennae. In this model the luminosity calculated under the assumption of isotropic emission is overestimated by a factor b which depends on the viewing angle and the physical parameters of the accretion disk (e.g. Madau, 1988; Urry et al. 1991).

King et al. (2001) proposed that one class of objects which may go through a phase of super Eddington accretion are close X-ray binaries experiencing a thermal timescale mass transfer episode: the atmosphere of the donor expands, over-filling its Roche lobe, and large amounts of material flow towards the compact companion, resulting in super-critical accretion. These episodes can be experienced by relatively early type stars when they evolve off the Main Sequence. However, in order to produce an observable XRB, the donor should not have a convective envelope (i.e. it should be earlier than A-type for a neutron star accretor) (A. King, private communication). Otherwise, the mass transfer episode will give rise to a common envelope binary. Although models show that super-Eddington accretion can also occur in common envelope X-ray binaries (Chevalier 1993, 1996; Fryer et al. 1996), the very large optical depths of the convective stellar atmospheres will make any produced X-ray emission unobservable, since it will be attenuated by absorption as well as scattering.

Recently Pacull & Mirioni (2002), based on the detection of high excitation lines in the optical spectrum of the ULX in the nearby galaxy Ho-II, suggest that the local ISM sees an ionizing continuum of $\sim 10^{40}$ erg s $^{-1}$ and hence the X-ray emission cannot be beamed. However, it is possible that highly ionized nebulae can also be produced by beamed X-ray binaries with the only difference that they would have a bi-conic morphology (similar to that of the ionization cones in Seyfert galaxies) if seen edge on. If seen face-on they should be indistinguishable from any nebulae ionized by an isotropic source.

3.2.3. ‘Runaway’ constraints to binary masses

In the beamed model, the positional offsets of the ULXs from the stellar clusters (Paper III) is explained easily by the runaway binary scenario. For beaming factors as low as 0.1, the mass of the compact object reduces to 1-10 M $_{\odot}$. Objects of this mass can easily receive large

kicks when their progenitor undergoes supernova explosion ($v \sim 100 - 30 \text{ km s}^{-1}$ respectively; Cordes & Chernoff 1998; Fryer & Kalogera, 2001) and be expelled from their parent clusters. The presence of these displacements, in the assumption that they are related to kicks, can help us further constrain the nature of the binary system.

The final velocity of the system depends both on the mass of the compact object and of the companion star. Rescaling from the Cordes & Chernoff (1998) kick velocities for neutron stars, we obtain $v = 245 * (M_{BH} + M_{comp})^{-1} \text{ km s}^{-1}$, where M_{BH} is the mass of the compact object and M_{comp} is the mass of the companion. In Fig. 7 we plot the timescale needed by the system to cover a distance of $\sim 300 \text{ pc}$ (which is the typical offset between the X-ray sources and their nearest optical counterparts; Paper III) as a function of the mass of the donor, for different masses for the compact object. Note that as discussed above, later than A type donors are excluded (hatched area). This is a limiting case for neutron star accretors; if the accretor is more massive then this limit moves to higher mass donors in order to avoid the formation of a transient source (King et al. 1996). Most high mass X-ray binaries enter their X-ray emitting phase soon after their donors evolve off the Main Sequence (e.g. Verbunt & van den Heuvel, 1995), therefore if the ULXs are HMXBs they should have been expelled from their parent clusters in a timescale comparable to the companion’s Main Sequence lifetime (Fig. 7). Imposing that the age of the companion should be at least similar to the timescale required by the system to move to its present position, results in an upper limit to the permitted donor masses given by the abscissa of the point where the Main Sequence lifetime– mass relation (dashed line) intercepts the solid lines in Fig. 7. Since the kick velocities can be much lower than those assumed for this plot, companions with lower masses would be consistent with the measured distances.

If the companion is too massive, the system would become active before it has an appreciable separation from its parent cluster; these massive binaries could be the counterparts of sources associated with star clusters. Alternatively, these objects could host massive IMBHs, as discussed in §3.2.1.

Fig. 7 suggests that sources with measured offset from a nearby star cluster (Paper III) may be binary systems with donor stars ranging from B2 to A type for a range of compact accretors from a 1.4 M_\odot neutron star to a 20 M_\odot black-hole. In these systems, super-Eddington accretion will lead to the formation of a thick accretion disk, as discussed earlier. This is not a problem even in the case of a magnetized neutron star (which may be common in young binaries), since polar accretion can well take place in the center of a thick accretion disk (A. King private communication). Moreover, the large magnetic fields may reduce the Thompson scattering cross-section and thus increase the Eddington limit (e.g. King et al. 2001). In the case of a strongly magnetized neutron star, one expects to observe strong cyclotron lines (as in pulsar binaries in our Galaxy; e.g. Nagase 1989) if the X-ray emission is produced close to the compact object. This could be a way of discriminating between black hole and pulsar accretors.

This model could also be used to connect the ULXs with the Galactic microquasars (e.g. Mirabel & Rodriguez

1999). As presented in Paper III, both types of sources have similar parameters for the disk black-body model used to fit their X-ray spectra, suggesting a similar structure in their accretion disks. In this case the factor of 10 difference in their luminosities may be explained in terms of different beaming factors. Indeed if microquasars accrete at lower rates than ULXs (but still super-Eddington,), the formed accretion disk will be slim (Abramowitz et al. 1988), in agreement with spectral fitting results (Watarai et al. 2000). This disk lacks the large funnel-like structure of thick disks, resulting in much lower beaming factors which however are still higher than in standard thin disks (e.g. Abramowitz et al. 1988). The lower accretion rates could be related to the details of the mass transfer and the orbital parameters of the binary. In this context at the upper end of the ULX population in the Antennae could be objects similar to those proposed by King et al. (2001), while lower luminosity sources could be similar to Galactic microquasars.

3.2.4. Effect of beaming on the XLF

Beaming has important implications for the observed XLF of the ULX population. Urry et al. (1991; see also Celotti et al. 1993) studied this effect in AGNs based on a calculation of the beaming factors for thick accretion disks orbiting supermassive black holes ($M \sim 10^8 \text{ M}_\odot$; Madau 1988). Their results apply to the XLF of the Antennae if the properties of the accretion disk (opening angle and size of the funnel, temperature structure and size of the disk) do not depend on the mass of the central object. They found that for a power-law parent luminosity function between luminosities l_1 and l_2 , the beamed XLF is flatter than the parent XLF from a luminosity L_1 (which is the minimum parent luminosity times the minimum beaming factor), up to a luminosity of $L_3 = A \cos(\theta_o) \times l_1$, where θ_o is the opening angle of the funnel. At higher luminosities the beamed XLF follows the same slope as the parent XLF (Fig. 8). The flattening of the XLF is due to absorption of the intrinsic (unbeamed) emission by the walls of the funnel when the line of sight is larger than θ_o (i.e. crosses the funnel). This behaviour is different than what one would expect for relativistic beaming where the intrinsic luminosity is just enhanced by a beaming factor. Since the slope of the parent XLF of the ULXs actually represents the mass function of the accreting objects, if they accrete at the same fraction of their Eddington rate, it could be used to constrain models for their formation.

Apart from the population of ULXs, a galaxy would have a population of normal XRBs (which may also have a power-law XLF; e.g. Sarazin et al. 2000; Tennant et al. 2001). Therefore, the total XLF for a galaxy would start at low L_X with a power-law with the slope of the underlying XRB population XLF and then flatten when the lowest luminosity ULXs appear, to finally assume the slope of the unbeamed population of the ULXs (dashed line in Fig. 8) at the critical luminosity which corresponds to the opening angle where the emission “funnel” can be observed. On the other hand if the Kording et al. (2001) model is valid, with X-ray binaries and ULXs having both beamed jets and unbeamed disk components such breaks would not be expected. Future more sensitive observations of the Antennae will extend the range of detected sources

well into the normal XRB regime and will allow us to test different scenarios.

From the maximum luminosity of the sources ($\sim 2 \times 10^{40}$ erg s $^{-1}$) and the maximum beaming factor predicted by Madau (1988) we can set an upper limit of $\sim 10 M_{\odot}$ on the maximum mass of the compact objects. This limit is fully consistent with stellar BHs. Since the mass of the compact object is $\sim 10 M_{\odot}$ we are in the regime of narrow mass distribution (case 2 of Urry et al. 1991). In this case the highest luminosity break is expected to occur at $\sim 3 \times 10^{39}$ erg s $^{-1}$, if the lowest mass compact object is a $1 M_{\odot}$ neutron star and assuming critical accretion. The shape of the XLF of the Antennae (figs 4,5) may be consistent with an excess of sources below $\sim 3 \times 10^{39}$ erg s $^{-1}$. In this model the first break should occur at $\sim 8 \times 10^{37}$ erg s $^{-1}$, just below our detection limit. The flattening of the XLF of ULXs between 10^{38} erg s $^{-1}$ and 10^{39} erg s $^{-1}$ may mask a possible break in the XLF of the normal binaries, due to the neutron star - black hole transition. This break should be close to the Eddington luminosity for a neutron star (e.g., Sarazin et al. 2000), and existing data suggest that is not present in star-forming galaxies (see Fig. 5). Therefore, XLFs extending to lower luminosities will allow us to test this model and constrain the low mass cutoff for the compact objects in the ULXs.

4. CONCLUSIONS

We have presented a study of the X-ray source population in the Antennae galaxies. We derive their luminosity function by taking into account effects related to the varying detection limit over the area of the galaxy and including count-rate and spectral uncertainties for each source. We find that the cumulative XLF has a slope ($\alpha = -0.45$), similar to that of the luminosity function of the star-forming galaxy M82 (Zezas et al. 2001) and the disk of the spiral M81 (Tennant et al. 2001). The XLF of the Antennae is instead much flatter than the XLF of early type galaxies and does not show a break around 3×10^{38} erg s $^{-1}$ as reported in the latter (e.g. Sarazin et al. 2001). These comparisons suggest that the dominant X-ray population in the Antennae is young. This conclusion agrees with the results of Paper III showing that almost all the optical counterparts of the X-ray sources in the Antennae are young stellar clusters and most of the radio counterparts have steep radio spectra, implying SNRs in the region. The comparison between the XLFs of different galaxies also indicates that more actively star-forming galaxies have larger numbers of ULXs, further associating these sources with star-formation activity and a young stellar population.

Our results suggest that $> 10-1000s M_{\odot}$ IMBH cannot be the sole explanation for all the ULXs in the Antennae, although they may explain a few of them. In particular, the general association of the ULXs with young star clus-

ters (Paper III) is hard to reconcile with the Taniguchi et al. (2000) formation scenario of IMBH, which requires long timescales. The displacement of the ULXs from neighboring young stellar clusters (Paper III), is hard to reconcile with the Portegies Zwart et al. (1999) model, but could be consistent with the Madau & Rees (2001) scenario, in which massive black holes may be the remnants of Population III stars, if these black holes capture a companion while crossing a dense star cluster. However, a more likely scenario may be that of runaway binaries with neutron stars or low-mass black holes which received kicks upon their formation.

Since it is unlikely that the majority of ULXs are powered by accretion onto an IMBH the only way to produce the observed luminosities is by supercritical accretion and the resulting beaming. Supercritical accretion (which is consistent with the X-ray spectral fits for ULXs) has as a natural consequence the formation of a funnel in the inner part of the accretion disk (e.g. Abramowicz et al. 1980), resulting in anisotropic emission (beaming; e.g. Madau 1980; King et al. 2001). Using the constraint provided by the displacement of the ULXs from the closest star clusters where they may have formed (Paper I.I), we derive masses of compact objects ranging from $1.4 M_{\odot}$ (neutron star) to $20 M_{\odot}$, and stellar companions of B3-A type. Only the few object found within a stellar cluster are likely to have a more massive counterpart.

The type of beaming produced by supercritical accretion would give a characteristic shape to the XLF, by producing two breaks, the position of which depends on the luminosity range of the parent population of the ULXs (or equivalently the mass range of the accretor). These breaks are not related either to the aging of the X-ray source population (e.g., Wu 2000, Kilgard et al. 2001) nor to the neutron star - black hole transition in the accretors of normal X-ray binaries (e.g. Sarazin et al. 2000). The flattening of the XLF of ULXs predicted by this model may mask any breaks associated with the normal XRB population. In the XLF of the Antennae we do not detect any break, but we are limited by the sensitivity of the present observation; future observations of the Antennae as well as other nearby star-burst galaxies, which will extend to lower luminosities, will allow us to test this model and set further constraints on the mass distribution of the accretors.

We thank the CXC DS and SDS teams for their efforts in reducing the data and developing the software used for the reduction (SDP) and analysis (CIAO). We thank Andrew King, Martin Elvis, Vicky Kalogera, Andrea Prestwich, Phil Kaaret and Jeff McClintock for useful discussions on these results. This work was supported by NASA contract NAS 8-39073 (CXC) and NASA Grant NAG 5-9983.

REFERENCES

Abramowicz, M. A., Czerny, B., Lasota, J. P., & Szuszkiewicz, E. 1988, ApJ, 332, 646
 Abramowicz, M. A., Calvani, M., & Nobili, L. 1980, ApJ, 242, 772
 Angelini, L., Loewenstein, M., & Mushotzky, R. F. 2001, ApJ, 557, L35
 Bauer, F. E., Brandt, W. N., Sambruna, R. M., Chartas, G., Garmire, G. P., Kaspi, S., & Netzer, H. 2001, AJ, 122, 182
 Bevington, P.R., & Robinson D.K., 1992, Data Reduction and Error Analysis for the Physical Sciences (McGraw Hill)
 Blanton, E. L., Sarazin, C. L., & Irwin, J. A. 2001, ApJ, 552, 106
 Cash, W. 1979, ApJ, 228, 939
 Celotti, A., Maraschi, L., Ghisellini, G., Caccianiga, A., & Maccacaro, T. 1993, ApJ, 416, 118
 Chevalier, R. A. 1996, ApJ, 459, 322

Chevalier, R. A. 1993, ApJ, 411, L33

Colbert, E. J. M. & Mushotzky, R. F. 1999, ApJ, 519, 89

Cordes, J. M. & Chernoff, D. F. 1998, ApJ, 505, 315

Crawford, D. F., Jauncey, D. L., & Murdoch, H. S. 1970, ApJ, 162, 405

Dobrzański, A., Ebeling, H., Glotfelty, K., Freeman, P., Damiani, F., Elvis, M., Calderwood, T., 2000, *Chandra* Detect 1.0 User Guide, http://asc.harvard.edu/ciao/documents_manuals.html

Fabian, A. C., Pringle, J. E., & Rees, M. J. 1975, MNRAS, 172, 15P

Fabbiano, G. 1988, ApJ, 325, 544

Fabbiano, G. 1989, Ann. Rev. Ast. Ap., 27, 87

Fabbiano, G. 1995, in X-ray Binaries, ed. W. H. G. Lewin, J. van Paradijs, & E. P. J. van den Heuvel (Cambridge: University Press), p. 390

Fabbiano, G., Zezas, A., & Murray, S. 2001, ApJ, 554, 1035 (Paper I)

Fender, R. P. 2001, MNRAS, 322, 31

Freeman P.E., Doe S. & Siemiginowska A., 2001, astro-ph/0108426

Fryer, C. L. & Kalogera, V. 2001, ApJ, 554, 548

Fryer, C. L., Benz, W., & Herant, M. 1996, ApJ, 460, 801

Gehrels, N. 1986, ApJ, 303, 336

Grimm J.H., Gilyanov M. & Sunyaev R. astro-ph 0109239

Irwin J.A., Sarazin C.L. & Bregman J.N., 2001 astro-ph/0107493

Kaaret, P., Prestwich, A. H., Zezas, A., Murray, S. S., Kim, D.-W., Kilgard, R. E., Schlegel, E. M., & Ward, M. J. 2001, MNRAS, 321, L29

Kennicutt, R. C. 1998, ApJ, 498, 541

Kilgard, R., Kaaret, P., Krauss, M., Prestwich, A. H., Raley, M. & Zezas, A., 2001, submitted to ApJ

King, A. R., Davies, M. B., Ward, M. J., Fabbiano, G., & Elvis, M. 2001, ApJ, 552, L109

King, A. R., Kolb, U., & Burderi, L. 1996, ApJ, 464, L127

Kording, E., Falcke, H. & Markoff, S., 2001, A&A, in press (astro-ph/0112385)

Kubota, A., Mizuno, T., Makishima, K., Fukazawa, Y., Kotoku, J., Ohnishi, T., & Tashiro, M. 2001, ApJ, 547, L119

La Parola, V., Peres, G., Fabbiano, G., Kim, D. W., & Bocchino, F. 2001, ApJ, 556, 47

Madau, P. & Rees, M. J. 2001, ApJ, 551, L27

Madau, P. 1988, ApJ, 327, 116

Makishima, K. et al. 2000, ApJ, 535, 632

Marston, A. P., Elmegreen, D., Elmegreen, B., Forman, W., Jones, C., & Flanagan, K. 1995, ApJ, 438, 663

Massey, P. & Hunter, D. A. 1998, ApJ, 493, 180

Matsumoto, H. & Tsuru, T. G. 1999, PASJ, 51, 321

Matsumoto, H., Tsuru, T. G., Koyama, K., Awaki, H., Canizares, C. R., Kawai, N., Matsushita, S., & Kawabe, R. 2001, ApJ, 547, L25

Miller, J. M., Fox, D. W., Di Matteo, T., Wijnands, R., Belloni, T., Pooley, D., Kouveliotou, C., & Lewin, W. H. G. 2001, ApJ, 546, 1055

Mirabel, I. F. & Rodríguez, L. F. 1999, ARA&A, 37, 409

Murdoch, H. S., Crawford, D. F., & Jauncey, D. L. 1973, ApJ, 183, 1

Nagase, F. 1989, PASJ, 41, 1

Portegies Zwart, S. F., Makino, J., McMillan, S. L. W., & Hut, P. 1999, A&A, 348, 117

Portegies Zwart, S. F. & McMillan, S. L. W., 2002, astro-ph/0201055

Prestwich, A., 2001, astro-ph/0108523

Primin, F. A., Forman, W., & Jones, C. 1993, ApJ, 410, 615

Ptak, A. & Griffiths, R. 1999, ApJ, 517, L85

Quinlan, G. D. & Shapiro, S. L. 1990, ApJ, 356, 483

Read, A. M., Ponman, T. J., & Strickland, D. K. 1997, MNRAS, 286, 626

Reynolds, C. S., Loan, A. J., Fabian, A. C., Makishima, K., Brandt, W. N., & Mizuno, T. 1997, MNRAS, 286, 349

Roberts T., & Warwick R., 2000, MNRAS, 315, 98

Sarazin, C. L., Irwin, J. A., & Bregman, J. N. 2000, ApJ, 544, L101

Sarazin, C. L., Irwin, J. A., & Bregman, J. N. 2001, ApJ, 556, 533

Stark, A. A., Gammie, C. F., Wilson, R. W., Bally, J., Linke, R. A., Heiles, C., & Hurwitz, M. 1992, ApJS, 79, 77

Supper, R., Hasinger, G., Lewin, W. H. G., Magnier, E. A., van Paradijs, J., Pietsch, W., Read, A. M., & Trümper, J. 2001, A&A, 373, 63

Taniguchi, Y., Shioya, Y., Tsuru, T. G., & Ikeuchi, S. 2000, PASJ, 52, 533

Tennant, A. F., Wu, K., Ghosh, K. K., Kolodziejczak, J. J., & Swartz, D. A. 2001, ApJ, 549, L43

Trinchieri, G. & Fabbiano, G. 1991, ApJ, 382, 82

Urry, C. M., Marziani, P., & Calvani, M. 1991, ApJ, 371, 510

Urry, C. M. & Shafer, R. A. 1984, ApJ, 280, 569

Van Speybroeck, L., Jerius D., Edgar, R. J., Gaetz, T. J., Zhao, P. & Reid, P. B. 1997, Proc. SPIE 3113, 89

Verbiest, G. & van den Heuvel 1995, in X-ray Binaries, ed. W. H. G. Lewin, J. van Paradijs, & E. P. J. van den Heuvel (Cambridge: University Press), p. 457

Wang, Q. D., Immler, S., & Pietsch, W. 1999, ApJ, 523, 121

Watarai, K., Fukue, J., Takeuchi, M., & Mineshige, S. 2000, PASJ, 52, 133

Watson M.G., 1990, in Windows on Galaxies, eds. G. Fabbiano, J.S. Gallagher and A. Renzini, 177 (Kluwer Academic Press)

Weisskopf, M., Tananbaum, H., Van Speybroeck, L. & O'Dell, S. 2000, Proc. SPIE 4012 (astro-ph 0004127)

Whitmore, B. C., Zhang, Q., Leitherer, C., Fall, S. M., Schweizer, F. ;, & Miller, B. W. 1999, AJ, 118, 1551

Wu, K., 2000, astro-ph/0103157

Yokogawa, J., Imanishi, K., Tsujimoto, M., Nishiuchi, M., Koyama, K., Nagase, F., & Corbet, R. H. D. 2000, ApJS, 128, 491

Zezas, A., Georgantopoulos, I. & Ward, M., 1999, MNRAS, 308, 302

Zezas A., Fabbiano G., Prestwich A., Ward M., & Murray S., 2001, Procs of The Central Kiloparsec of Starbursts and AGN: The La Palma Connection, ASP Conf Series, Vol. 249, 425, Eds. J.H. Knapen, J.E. Beckman, I. Shlosman, and T.J. Mahoney (astro-ph/0109302)

Zezas, A., Fabbiano, G., Rots, A., & Murray, S., 2001a, submitted to ApJS(Paper II)

Zezas, A., Fabbiano, G., Rots, A., & Murray, S., 2001b, submitted to ApJ(Paper II)

TABLE 1
ASSUMED MODELS FOR THE CALCULATION OF THE LUMINOSITY FUNCTION

Luminosity range (1)	Photon index (2)	Column density (3)
$< 3 \times 10^{38}$	3.36 ± 1.5	0.28 ± 0.5
$3 \times 10^{38} - 10^{39}$	3.37 ± 1.0	0.23 ± 0.15
$> 10^{39}$	1.7 ± 0.5	0.1 ± 0.07

FIG. 1.— The uncorrected luminosity histogram of all the sources in the Antennae, compared with the uncorrected luminosity histogram of the point-like and unobscured sources (hatched area), which we use to derive the XLF in this paper.

FIG. 2.— An image of the 0.3-10.0 keV diffuse background in the Antennae galaxies as calculated by the *wavdetect* tool (see Paper II). The detected sources are marked by their 3σ positional ellipses. The contours correspond to levels of 0.1, 0.15 and 0.35 counts/pixel. Sources outside the second contour (0.15counts/pixel) formed the Low background XLF, sources between the second and the third contour formed the Medium background XLF while sources inside the third contour formed the High background XLF.

FIG. 3.— Left (a):The uncorrected (solid line) and corrected (dash-dot line) luminosity distribution of sources found in the three different background environments. Right (b): The correction function for these three background levels. Triangles correspond to the high background, squares to medium background and stars to low background levels. The dashed line shows the 50% completeness limit for all curves.

FIG. 4.— Top panel: Left (a): The completeness corrected differential XLF of all the sources in the Antennae. Right (b): The cumulative XLF of the sources in the Antennae, together with the best fit power-law (solid line) and the residuals (in number of sources) after the fit. Bottom panel: The differential (left; c) and cumulative (right; d) XLF of the point sources in the Antennae from a Monte Carlo simulation which takes into account errors associated with count-rate and spectral uncertainties. Together with the cumulative XLF we show the best fit power-law (solid line) and the residuals (in number of sources) after the fit.

FIG. 5.— Comparison between the luminosity functions of Antennae (this work), M82 (Zezas et al. 2001), the disk of M81 (Tennant et al. 2001) and NGC4697 (Sarazin et al. 2001). The dashed line shows the XLF of the Antennae for $H_0 = 75 \text{ km s}^{-1} \text{ Mpc}^{-1}$. We also plot the XLFs of the HMXB and the LMXB population of the Galaxy (Grimm et al. 2001).

FIG. 6.— Comparison between the slopes of the cumulative luminosity functions of star-forming (Antennae, M82, the disk of M81) and early type galaxies (NGC4697, NGC1553, and the bulge of M31). The ordinate is the logarithm of the normalization of the XLF at $10^{38} \text{ erg s}^{-1}$. Data are from: this work (Antennae); Zezas et al. 2001 (M82); Tennant et al. 2001 (M81); Sarazin et al. 2001 (NGC 4697); Blanton et al. 2001 (NGC1553), Primini et al. 1993 (M31).

FIG. 7.— A plot of the time required by a binary system of various compact object masses (given in the end of the solid line) to reach a distance of 300 pc as a function of the donor mass (solid lines). The top and right axes give the spectral types corresponding to each donor mass and Main Sequence lifetime. The dashed line shows the Main Sequence lifetime - mass relation. The permitted donor types are given by the thick part of the solid lines. The hatched area shows the region of donors with convective envelopes, which would not produce an observable XRB, according to the model of King et al. (2001) (see text).

FIG. 8.— An illustration of the effect of beaming on the parent differential XLF of black holes with thick accretion disks (adopted from Urry et al. 1991). L_1 corresponds to the minimum observed luminosity for a thick accretion disk and L_3 corresponds to the position of the break in the beamed XLF. The normalizations of the XLFs and the slopes of the non ULX and parent XLFs are arbitrary.

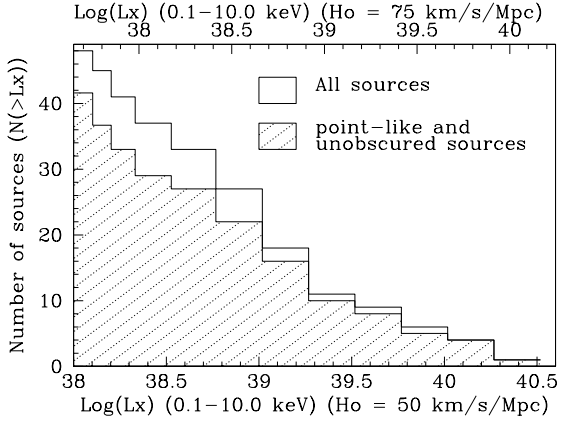


FIG. 1.—

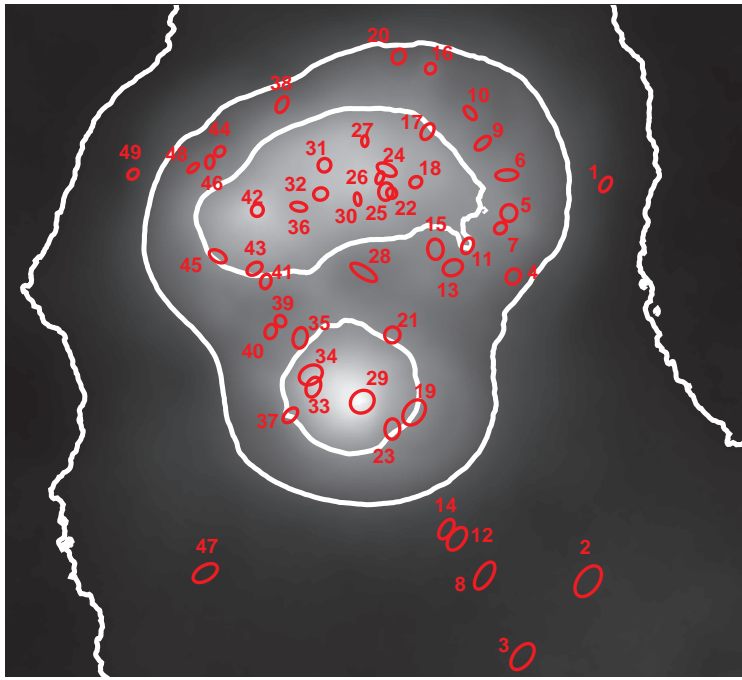


FIG. 2.—

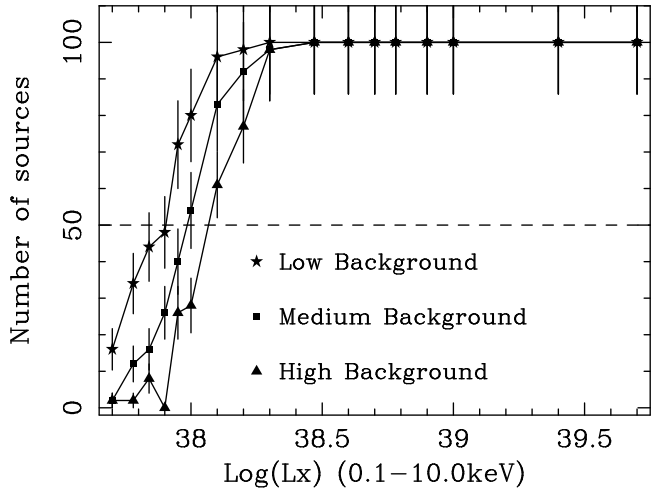
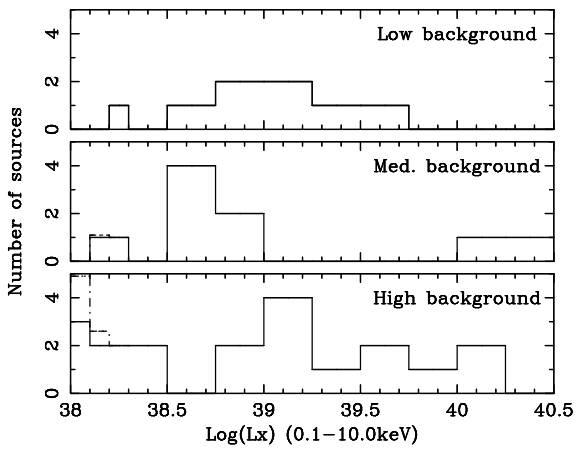


FIG. 3.—

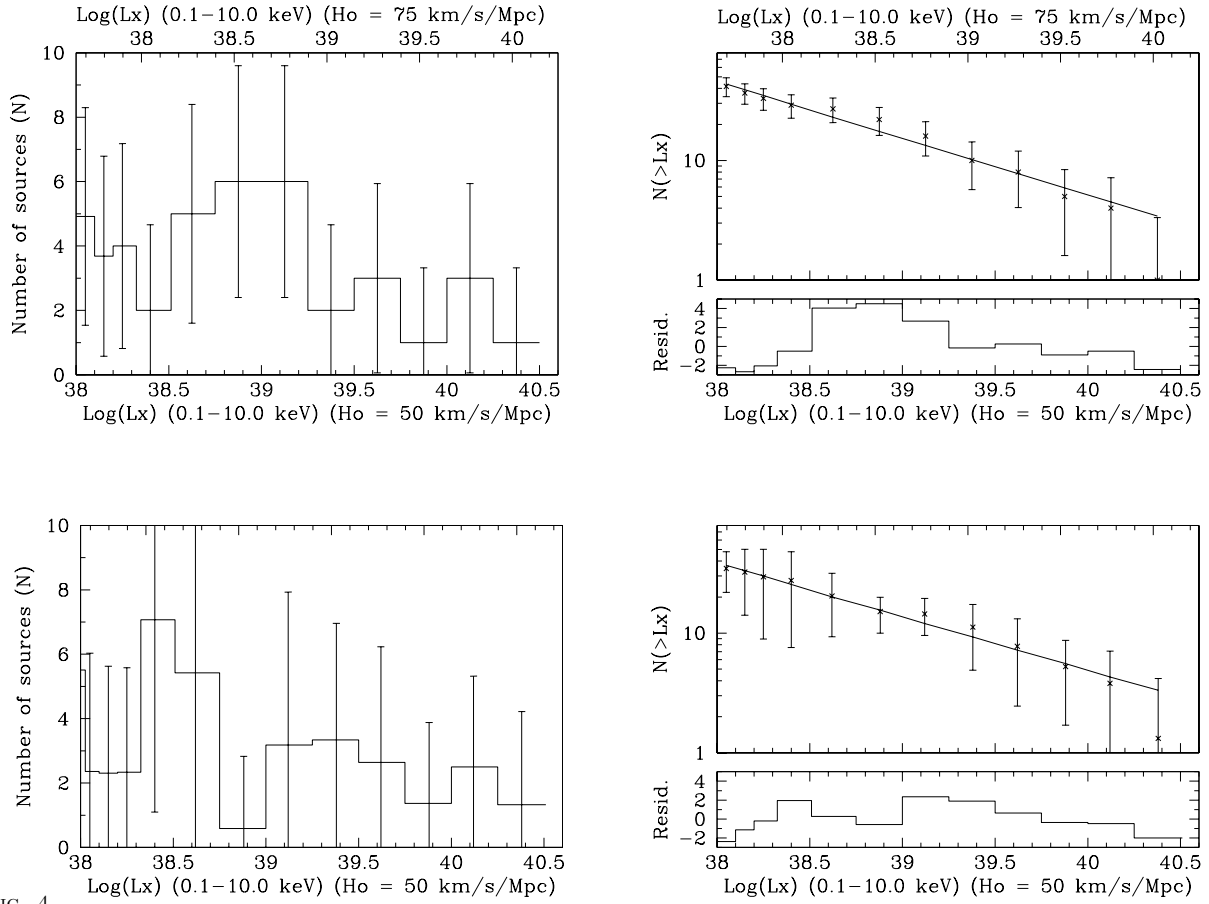


FIG. 4.—

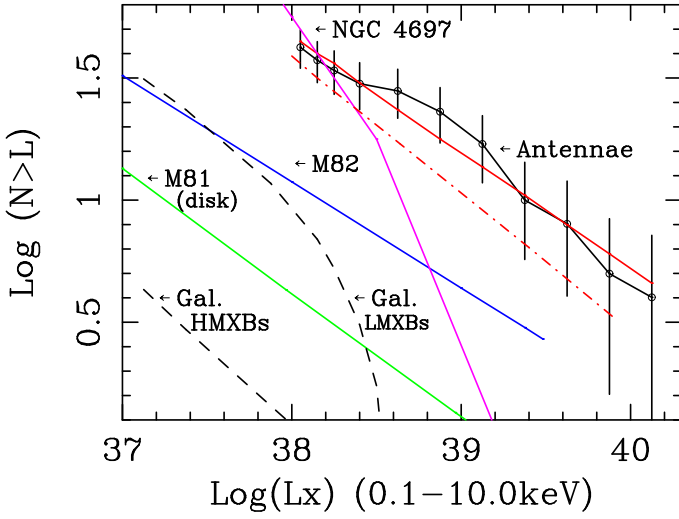


FIG. 5.—

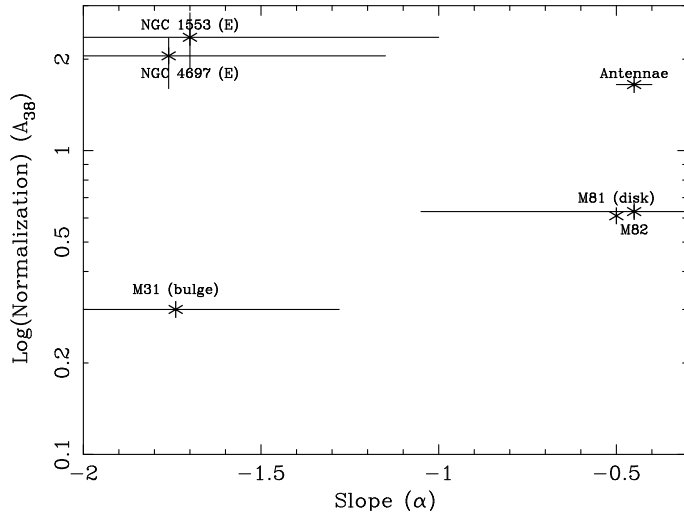


FIG. 6.—

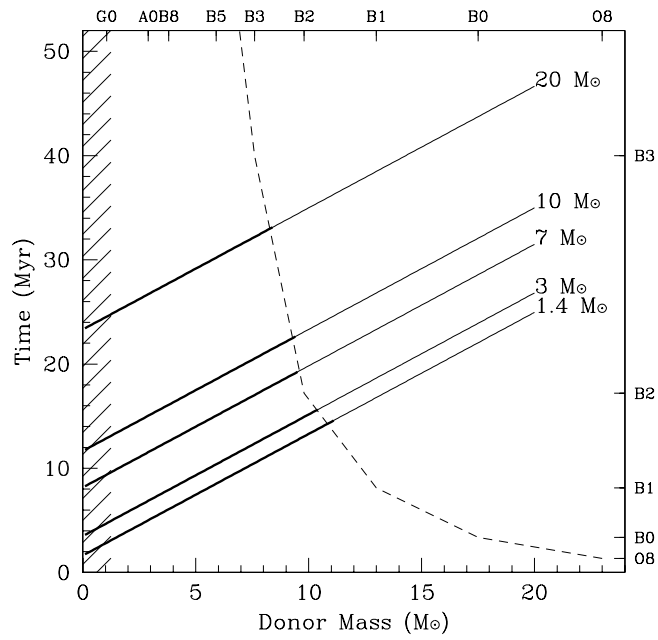


FIG. 7.—

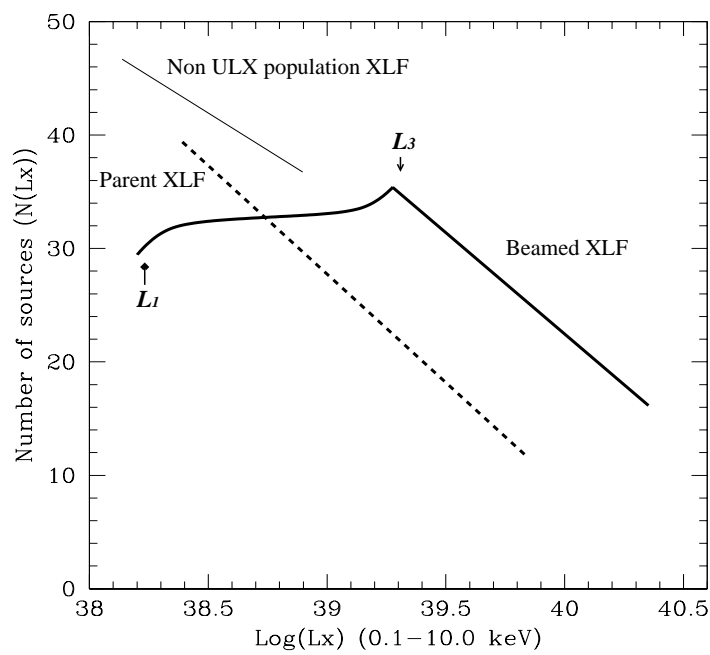


FIG. 8.—